Algorithm for constructing the compact transfer matrix for 1-D structures possessing singular coupling Hamiltonian sub-blocks.

D. Areshkin and C. White

Naval Research Laboratory, Code 6180, 1555 Overlook Ave, Washington, DC 20375

ABSTRACT

We present the algorithm for the construction of the transfer matrix, associated with the Hamiltonian of the arbitrary one-dimensional structure possessing translational or screw symmetry. The advancement of our technique is three-fold. First, it allows to handle arbitrarily singular Hamiltonian sub-blocks, which are likely to appear in the 1-D structures with screw symmetry. Secondly, it produces the transfer matrixes, which have only non-zero eigenvalues. That means the transfer matrixes are of the smallest possible size and hence have maximum computational efficiency. And finally, the absence of zero eigenvalues greatly enhances the numerical precision. To demonstrate the utility of the method we examine the conductance of (10,7) and (8,8) nano-tubes as the function of the bending angle using Landauer's formalism with Environment-Dependent Tight-Binding [Tang *et al.*, Phys. Rev. B **53**, 979 (1996)] and its self-consistent extension [Areshkin *et al.*, J. Phys.: Condens. Matter **16** 6851 (2004)]. With minor difference both methods indicate that the nano-tube conductance is very stable with respect to bending. The appearance of the kink does not appreciably deteriorate the conductance up to the point when the opposite sides of the nanotube in the kink region begin to interact with each other. At that point the small increase of the bending angle, which is 60° for both tube types, triggers the abrupt decrease of the conductance. Further bending up to 120° does not have much effect on the conductance, which constitutes approximately 25% and 70% from the ideal value for (10,7) and (8,8) nano-tubes respectively. The self-consistent model indicates mild charge depletion (~0.1 electron charge) in the kink area.

I. INTRODUCTION

The popular application of the transfer matrix technique is the solution of the problem associated with the Schrödinger eigensystem equation

$$H\left[\lambda_i\right]\cdot c_i = \varepsilon\, c_i\,. \tag{1}$$

The task is to find all possible scalars λ_i and associated eigenvectors c_i for the *given* value of ε. Matrix $H[\lambda]$ depends on λ as

$$H\left[\lambda\right] = h^{(0)} + \sum_{n=1}^{M}\left(h^{(n)T}\,\lambda^{-n} + h^{(n)}\,\lambda^{n}\right)\,, \tag{1-a}$$

where $h^{(n)}$ are known square $m\times m$ matrixes. Solution of Eq.(1) is the essential part of the algorithm for the construction of the Green's functions as it is explained in the previous paper. The standard way to handle the problem is to assemble the transfer matrix $\mathbf{T}[\varepsilon]$, such that some or all of its eigenvalues correspond to the set $\{\lambda_i\}$, which satisfies Eq.(1). The set of vectors $\{c_i\}$ is constructed from the corresponding eigenvectors of matrix **T**. When $h^{(n)}$ (n = 1,…M) are non-singular the construction of **T** is straightforward.[1,2] In that case the size of matrix **T** is 2 M m, and all **T** eigenvalues coincide with the set $\{\lambda_i\}$. Vectors c_i can be chosen as the first m components of the corresponding eigenvectors of **T**.

However, non-singular $h^{(n)}$ is more an exception than a rule. The first attempt to resolve the problem associated with the singular $h^{(n)}$ has been undertaken by Chang and Schulman.[1] Their method was formulated for the special type of singularity inherent to the coupling between crystalline planes. That was not considered a deficiency of the method, because it was adequate for the physical problem in hand. However, with the advent of 1-D quantum wires, this shortcoming became noticeable, since the singularity structure of the coupling matrixes associated with 1-D Hamiltonian does not generally match any regular pattern and cannot be handled with the Chang and Schulman's algorithm. The singularity issue has been recently addressed by Tomfohr and Sankey[2] who have developed the transfer matrix technique for an arbitrary singular $h^{(M)}$, but with the constraints on the singularity type of matrix $h^{(i)}$ for $i < M$. Even with such restriction the Tomfohr and Sankey method formally solves the singularity problem (except the pathological case discussed later) because one can always increase the size of the unit cell in

such way that the Hamiltonian for 1-D structure assumes tri-block-diagonal form. In that case $M = 1$ and Eq.(1-a) transforms to

$$H_{SC}[\lambda] = h_{SC}^{(0)} + h_{SC}^{(1)T}\ \lambda^{-1} + h_{SC}^{(1)}\ \lambda\ , \tag{1-b}$$

where matrix $h_{SC}^{(1)}$ can be arbitrarily singular (subscript *SC* stands for super-cell). As it will be explained shortly the transformation (1-b) can be the adequate remedy only for small matrixes H_{SC} and (or) for the Hamiltonian models with the energy spectrum lying within a reasonably small range, e.g. the π-orbital tight-binding Hamiltonian used in the previous paper, which eigenvalues span from –8.1 eV to +8.1 eV. At the same time our experience with the problem described in section VII indicates that machine precision is by far insufficient to obtain $\{\lambda_i\}$ and $\{c_i\}$ using Tomfohr-Sankey's method in conjunction with Eq.(1-b). To compensate for the poor numerical performance of this method we had to use at least 40 significant digits for the floating numbers representation.

We present the algorithm for the construction of the transfer matrix **T** associated with 1-D structures possessing translational or screw symmetry. The practical difference between our method and the algorithm devised by Tomfohr and Sankey is twofold. First, our method can handle singular Hamiltonian sub-block matrixes $h^{(i)}$ for $i = 1...M$. This issue is important because the situation when matrixes $h^{(i)}$ $(0 < i < M)$ may be singular or even zero is common for 1-D structures with screw symmetry. For example, consider the helical motif of carbon nano-tube, which consists from only two adjacent atoms. Sub-blocks $h^{(i)}$ describes interaction between helical motifs with indexes i and 0. The nearest neighbor of the motif with index 0 has index i_1, which corresponds to one "almost complete" revolution along the spiral associated with the nano-tube screw symmetry. For the large diameter nano-tubes some helical motifs (e.g. diametrically opposite to the 0-th cell) with indexes between 0 and i_1 may have no interaction with cell 0, and hence zero $h^{(i)}$.

The second principle advantage of our method is the handling of non-physical **T** eigenvalues. Tomfohr and Sankey construct **T** matrix in such way that all non-physical eigenvalues are substituted by zeros. On the contrary, our algorithm produces the transfer matrix of the smallest possible size, which means that **T** does not have non-physical zero eigenvalues. Besides faster eigenproblem computation this aspect provides substantial advantage for the numerical stability of our method. In a multi-band tight-binding or

DFT models the energy range of the allowed states spans over several tens of eV. The larger is the difference between the sampling energy and the allowed energy for the most remote energy band, the smaller is the minimal eigenvalue of **T**. For every eigenvalue λ_i corresponding to the exponentially decaying state ($|\lambda_i| < 0$), there exists the eigenvalue λ_i^{-1}, which corresponds to the exponentially growing state. Therefore, if $|\lambda_{min}|$ is the smallest non-zero eigenvalue, the condition number of **T** is $\kappa = |\lambda_{max}| / |\lambda_{min}| = |\lambda_{min}|^{-2}$. For the valence electron model it is not uncommon to have κ up to 10^8 (κ is expected to be substantially larger for all-electron model). For such κ the eigenvalue problem can be still handled by using machine precision. However, if **T** additionally has true zero eigenvalues, the numerical precision of the eigenproblem solution deteriorates due to the mixing between the true null-space eigenvectors and the eigenvectors corresponding to small non-zero λ's. Non-physical zero eigenvalues, which appear as small non-zero numbers in the numeric solution, are difficult to separate from the actual small non-zero λ's. Separation criterion is hard to systemize because it depends on system size, singularity pattern, basis set, energy range and other parameters.

To exemplify the utility of **T** matrix algorithm we perform the computation of the conductance through the bent (10,7) and (8,8) nano-tubes for the bending angle ranging from 0° to 120°. The transfer matrix is used for the self-energy computation as it is explained in the previous paper. We evaluate the conductance using Landauer's formalism with Environment-Dependent Tight-Binding[3] and its self-consistent extension.[4,5] The conductance for both tubes appears to have very little sensitivity for bending up to the angle of approximately 60°, when the opposite sides of the tube's surface in the kink region begin to interact with each other. Beyond that point the conductance for (10,7) and (8,8) nano-tubes differs substantially: for both nano-tube types the conductance does not have strong angular dependence, but its value constitutes approximately 70% from the ideal conductance for (8,8) nano-tube, and only 25% for (10,7) nano-tube.

The remainder of this paper is organized as follows. The next section contains definitions related to the description of the Hamiltonian associated with the infinite 1-D structure. Section III outlines the route we use to attack the problem. Sections IV-V are the core part of the paper, which contains the description of the algorithm for the transfer matrix construction. Section VI contains brief step-by-step summary of the algorithm.

Finally, in section VII we demonstrate the application of the transfer matrix technique to the nano-tube conductance simulation.

II. HAMILTONIAN DESCRIPTION

In the atomic orbital representation the infinite Hamiltonian matrix H_∞ associated with an arbitrary 1-D structure possessing screw or translational symmetry has band-diagonal form. For certainty in the following we consider orthogonal basis set Hamiltonian with 7 bands. Equation (2) shows the portion of the infinite Hamiltonian matrix

$R^{-3}H_2^TR^3$	$R^{-2}H_1^TR^2$	$R^{-1}H_0R^1$	$R^{-1}H_1R^1$	$R^{-1}H_2R^1$	$R^{-1}H_3R^1$	0	0	0
$R^{-3}H_3^TR^3$	$R^{-2}H_2^TR^2$	$R^{-1}H_1^TR^1$	H_0	H_1	H_2	H_3	0	0
0	$R^{-2}H_3^TR^2$	$R^{-1}H_2^TR^1$	H_1^T	$R^1H_0R^{-1}$	$R^1H_1R^{-1}$	$R^1H_2R^{-1}$	$R^1H_3R^{-1}$	0
0	0	$R^{-1}H_3^TR^1$	H_2^T	$R^1H_1^TR^{-1}$	$R^2H_0R^{-2}$	$R^2H_1R^{-2}$	$R^2H_2R^{-2}$	$R^2H_3R^{-2}$
0	0	0	H_3^T	$R^1H_2^TR^{-1}$	$R^2H_1^TR^{-2}$	$R^3H_0R^{-3}$	$R^3H_1R^{-3}$	$R^3H_2R^{-3}$

(2)

In the given example the entire Hamiltonian matrix can be obtained from the four sub-blocks H_0, H_1, H_2, H_3, and the orbital rotation matrix R (which is unity in the case of translational symmetry). H_0 is associated with the interaction between the atomic orbitals within the unit cell with index 0, and H_i ($i > 0$) represent the interaction between the unit cells with indexes 0 and i. Unit cell may contain more than one helical motifs, which are the smallest irreducible building blocks stipulated by the symmetry of the molecular structure. As it will be explained in the next section, the fewer helical motifs are contained in the unit cell the better is the numerical stability of the transfer matrix eigenproblem.

Matrix R has the same size as H_i, and is defined as follows. Let us denote the coordinate system associated with the unit cell at the origin ($i = 0$) as $\boldsymbol{CS_0}$, and the coordinate system associated with the unit cell with index 1 as $\boldsymbol{CS_1}$. $\boldsymbol{CS_1}$ is rotated by the screw angle with respect to $\boldsymbol{CS_0}$. Matrix R transforms the portion of the wave vector associated with unit cell 1 in $\boldsymbol{CS_1}$ to the wave vector coefficients in $\boldsymbol{CS_0}$. R is unitary and real because we assume real atomic orbital basis set. Therefore $R^{-1} = R^{\mathrm{T}}$. The Bloch theorem

for 1-D systems with screw symmetry can be used as another possible way to define R. For any given energy and k-number the state vector for the infinite system is:

$$C_i^{\infty} \equiv \begin{pmatrix} \vdots \\ R^{-2} \cdot c_i^{(0)} \times \lambda_i^{-2} \\ R^{-1} \cdot c_i^{(0)} \times \lambda_i^{-1} \\ c_i^{(0)} \\ R^{1} \cdot c_i^{(0)} \times \lambda_i^{1} \\ R^{2} \cdot c_i^{(0)} \times \lambda_i^{2} \\ \vdots \end{pmatrix} \equiv \begin{pmatrix} \vdots \\ R^{-2} \cdot c_i^{(-2)} \\ R^{-1} \cdot c_i^{(-1)} \\ c_i^{(0)} \\ R^{1} \cdot c_i^{(1)} \\ R^{2} \cdot c_i^{(2)} \\ \vdots \end{pmatrix} , \qquad (3)$$

where $\lambda_i = Exp[i\,k_i]$. Vectors … $c_i^{(-2)}$, $c_i^{(-1)}$, $c_i^{(0)}$, $c_i^{(1)}$, $c_i^{(2)}$, … are associated with respective unit cells and have the same size as Hamiltonian sub-blocks H_i.

Besides the notions of unit cell and helical motif we will be using the supercell partition of 1-D structure, which brings Hamiltonian matrix to the tri-block-diagonal form. Lines in Eq.(2) mark such tri-block-diagonal partition. The number of the unit cells in the supercell always equals the number of sub-blocks H_i minus one, which is three in our example. We assume the following notation for the Hamiltonian sub-blocks associated with the supercell

$$H_{SC} = \begin{pmatrix} H_0 & H_1 & H_2 \\ H_1^T & R^1 H_0 R^{-1} & R^1 H_1 R^{-1} \\ H_2^T & R^1 H_1^T R^{-1} & R^2 H_0 R^{-2} \end{pmatrix} \quad \tau_{SC} = \begin{pmatrix} H_3 & 0 & 0 \\ R^1 H_2 R^{-1} & R^1 H_3 R^{-1} & 0 \\ R^2 H_1 R^{-2} & R^2 H_2 R^{-2} & R^2 H_3 R^{-2} \end{pmatrix} \qquad (4)$$

Then, it is easy to see that the left supercell in Eq.(2)

$$\begin{pmatrix} R^{-3} H_3^T R^3 & R^{-2} H_2^T R^2 & R^{-1} H_1^T R^1 \\ 0 & R^{-2} H_3^T R^2 & R^{-1} H_2^T R^1 \\ 0 & 0 & R^{-1} H_3^T R^1 \end{pmatrix} = R_{SC}^{-1} \cdot \tau_{SC}^T \cdot R_{SC}^1 ,$$

where R_{SC} is the supercell rotation matrix:

$$R_{SC} = \begin{pmatrix} R^M & 0 & 0 \\ 0 & R^M & 0 \\ 0 & 0 & R^M \end{pmatrix} . \qquad (5)$$

The power M and the number of R^M sub-blocks in Eq.(5) equals to the number of the unit cells in the supercell; in our example $M = 3$. In the terms of the supercell sub-blocks Eq.(2) for the Hamiltonian matrix transforms to:

$$H_\infty = \left(\begin{array}{c|c|c|c|c} \ddots & \ddots & 0 & \vdots & \iddots \\ \hline \ddots & R_{SC}^{-1}\cdot H_{SC}\cdot R_{SC}^{1} & R_{SC}^{-1}\cdot \tau_{SC}\cdot R_{SC}^{1} & 0 & \cdots \\ \hline 0 & R_{SC}^{-1}\cdot \tau_{SC}^{T}\cdot R_{SC}^{1} & H_{SC} & \tau_{SC} & 0 \\ \hline \cdots & 0 & \tau_{SC}^{T} & R_{SC}^{1}\cdot H_{SC}\cdot R_{SC}^{-1} & \ddots \\ \hline \iddots & \vdots & 0 & \ddots & \ddots \end{array}\right) \qquad \text{(2-a)}$$

The analog of Eq.(3) for the state vector in the supercell notation is:

$$C_i^{\infty} \equiv \begin{pmatrix} \vdots \\ R_{SC}^{-2}\cdot C_i^{(0)}\times\Lambda_i^{-2} \\ R_{SC}^{-1}\cdot C_i^{(0)}\times\Lambda_i^{-1} \\ C_i^{(0)} \\ R_{SC}^{1}\cdot C_i^{(0)}\times\Lambda_i^{1} \\ R_{SC}^{2}\cdot C_i^{(0)}\times\Lambda_i^{2} \\ \vdots \end{pmatrix} \equiv \begin{pmatrix} \vdots \\ R_{SC}^{-2}\cdot C_i^{(-2)} \\ R_{SC}^{-1}\cdot C_i^{(-1)} \\ C_i^{(0)} \\ R_{SC}^{1}\cdot C_i^{(1)} \\ R_{SC}^{2}\cdot C_i^{(2)} \\ \vdots \end{pmatrix} , \qquad \text{(3-a)}$$

where $\Lambda_i = \lambda_i^M$. Vectors … $C_i^{(-2)}$, $C_i^{(-1)}$, $C_i^{(0)}$, $C_i^{(1)}$, $C_i^{(2)}$, … are associated with respective supercells and have the same size as Hamiltonian supercell sub-blocks H_{SC} and τ_{SC}.

The infinite Schrödinger equation $H_\infty \cdot C_\infty = \varepsilon \times C_\infty$ can be transformed to the finite size eigenproblem by dot-multiplication of Eqs.(2) and (3). The multiplication of the sub-block row associated with the unit cell 0 in Eq.(2) by state vector from Eq.(3) results in Eq.(6):

$$\begin{aligned} &\lambda_i^{-3}R^{-3}H_3^T R^3 R^{-3}c_i^{(0)} + \lambda_i^{-2}R^{-2}H_2^T R^2 R^{-2}c_i^{(0)} + \lambda_i^{-1}R^{-1}H_1^T R^1 R^{-1}c_i^{(0)} + \\ &H_0 c_i^{(0)} + \lambda_i^1 H_1 R^1 c_i^{(0)} + \lambda_i^2 H_2 R^2 c_i^{(0)} + \lambda_i^3 H_3 R^3 c_i^{(0)} = \varepsilon \times c_i^{(0)} \end{aligned} \qquad (6)$$

The compact form of Eq.(6) is:

$$H[\lambda_i]\cdot c_i^{(0)} = \varepsilon \times c_i^{(0)} , \qquad \text{(7-a)}$$

which is identical to Eq.(1). Here $H[\lambda]$ is given by Eq.(1-a), and $h^{(n)} = H_i \cdot R^n$. In the following $\{c_i^{(0)}\}$ denotes the set of all possible vectors $c_i^{(0)}$, which are the solutions of Eq.(7-a) associated with the respective finite non-zero λ_i from the set $\{\lambda_i\}$. For the super-cell the equation analogous to Eq.(7) has the form:

$$H[\Lambda_i]\cdot C_i^{(0)} = \varepsilon \times C_i^{(0)} , \qquad \text{(7-b)}$$

where

$$H[\Lambda] = \Lambda^{-1}\left(\tau_{SC} \cdot R_{SC}\right)^{T} + H_{SC} + \Lambda\, \tau_{SC} \cdot R_{SC} \ . \tag{8}$$

$\{C_i^{(0)}\}$ denotes the set of all possible solutions of Eq.(7-b), which are associated with the respective finite non-zero Λ_i from the set $\{\Lambda_i\}$, and $\{C_i^{(-1)}\}$ denotes the set of vectors obtained from $\{C_i^{(0)}\}$ through multiplying it by respective inverse Λ_i: $C^{(-1)}{}_i = C^{(0)}{}_i\, \Lambda_i^{-1}$. For the future reference we define the set of vectors $\{C^{\times 2}\}$, which is composed from joined vectors $C^{(-1)}{}_i$ and $C^{(0)}{}_i$. The number of vectors in $\{C^{\times 2}\}$ is the same as in $\{C^{(-1)}\}$ or $\{C^{(0)}\}$, but the vector length is two times larger, and equals twice the size of τ_{SC}.

III. SOLUTION OUTLINE

The construction of the transfer matrix **T** is performed in two steps. First we show how to construct the minimal size transfer matrix $\mathbf{T_{SC}}$ for the supercell, such that $\mathbf{T_{SC}}$ does not have non-physical eigenvalues. Theoretically $\mathbf{T_{SC}}$ can be used to solve the eigenproblem, and its eigenvectors $\{C^{\times 2}\}$ and eigenvalues $\{\Lambda_i\}$ can be utilized for the construction of the Green's function. In practice, however, $\mathbf{T_{SC}}$ is often ill-conditioned, and is not suitable for numeric eigenproblem solution. That usually happens when the number of the unit cells M in the supercell is too large. Since $|\Lambda_{\min}| = |\lambda_{\min}|^{M}$, the condition number κ_{SC} of $\mathbf{T_{SC}}$ equals $|\Lambda_{\min}|^{-2} = |\lambda_{\min}|^{-2\,M} = \kappa^{M}$, i.e. $\mathbf{T_{SC}}$ is substantially more ill-conditioned than **T**. Therefore it is more practical to work with matrix **T** rather than $\mathbf{T_{SC}}$. The role of $\mathbf{T_{SC}}$ is to show how to build the "contracted" vector space $\{D^{\times 2}{}_i\}$, which is reversibly mapped on $\{C^{\times 2}{}_i\}$: $\{C^{\times 2}{}_i\} \leftrightarrow \{D^{\times 2}{}_i\}$. The number of vectors in $\{D^{\times 2}{}_i\}$ equals the length of the vectors $D^{\times 2}{}_i$ and equals the number of vectors in $\{C^{\times 2}{}_i\}$. The eigenvalues of matrix $\mathbf{T_{SC}}$ constructed in $\{D^{\times 2}{}_i\}$ space are the same as all possible finite non-zero solutions of Eq.(7-b). After the transformation matrix X for $\{C^{\times 2}{}_i\} \xleftrightarrow{X} \{D^{\times 2}{}_i\}$ mapping is obtained it is used to build the transfer matrix **T** in $\{D^{\times 2}{}_i\}$ space. The eigenvalues $\{\lambda_i\}$ of the transfer matrix **T** are all possible finite non-zero solutions of Eq.(7-a).

IV. CONSTRUCTION OF $\mathbf{T_{SC}}$

Equations (7-b) and (8) can be combined as:

$$\left(\tau_{SC}\cdot R_{SC}\right)^{T}\cdot C_i^{(-1)}+\left(H_{SC}-\varepsilon\times I\right)\cdot C_i^{(0)}+\left(\tau_{SC}\cdot R_{SC}\right)\cdot C_i^{(1)}=0, \tag{9}$$

where I is identity matrix. We use singular value decomposition to represent $(\tau_{SC}\cdot R_{SC})^{\mathrm{T}}$ and $(\tau_{SC}\cdot R_{SC})$:

$$\begin{aligned}&\left(\tau_{SC}\cdot R_{SC}\right)=U\cdot W\cdot V^{T}\\&\left(\tau_{SC}\cdot R_{SC}\right)^{T}=V\cdot W\cdot U^{T}\\&W=\begin{pmatrix}W_D & 0\\ 0 & 0\end{pmatrix}\end{aligned} \tag{10}$$

Here U and V are real unitary matrixes, and W_D is nonsingular diagonal matrix, which size equals the size of τ_{SC} minus the size of null-space of τ_{SC}. Taking into account that $C_i^{(1)} = \Lambda_i\, C_i^{(0)}$ Eqs.(9-10) can be combined as:

$$U^{T}\cdot V\cdot W\cdot U^{T}\cdot C_i^{(-1)}+U^{T}\cdot\left(H_{SC}-\varepsilon\times I\right)\cdot V\cdot V^{T}\cdot C_i^{(0)}=-\Lambda_i\times W\cdot V^{T}\cdot C_i^{(0)}. \tag{11}$$

Defining

$$\begin{aligned}&D_i^{(-1)}=U^{T}\cdot C_i^{(-1)},\quad D_i^{(0)}=V^{T}\cdot C_i^{(0)},\\&F=U^{T}\cdot V,\quad Y=U^{T}\cdot(H_{SC}-\varepsilon\times I)\cdot V,\end{aligned} \tag{12}$$

we rewrite $C_i^{(0)} = \Lambda_i\, C_i^{(-1)}$ as:

$$F\cdot D_i^{(0)}=\Lambda_i\times D_i^{(-1)}\ . \tag{13}$$

Using definitions (12) Eq. (11) can be rewritten as:

$$F\cdot W\cdot D_i^{(-1)}+Y\cdot D_i^{(0)}=-\Lambda_i\times W\cdot D_i^{(0)}. \tag{14}$$

Next we partition all matrixes in four sub-locks in such way that the upper-left corner sub-matrix is of the same size as W_D, which means that the size of the low-right corner sub-matrix equals to the size of the null-space of τ_{SC}. Vectors $D_i^{(-1)}$ and $D_i^{(0)}$ are partitioned in the similar way: the upper portion of the vector is of the same size as W_D.

$$\begin{pmatrix}F_{11} & F_{12}\\ F_{21} & F_{22}\end{pmatrix}\cdot\begin{pmatrix}W_D & 0\\ 0 & 0\end{pmatrix}\cdot\begin{pmatrix}D1_i^{(-1)}\\ D2_i^{(-1)}\end{pmatrix}+\begin{pmatrix}Y_{11} & Y_{12}\\ Y_{21} & Y_{22}\end{pmatrix}\cdot\begin{pmatrix}D1_i^{(0)}\\ D2_i^{(0)}\end{pmatrix}=-\Lambda_i\times\begin{pmatrix}W_D & 0\\ 0 & 0\end{pmatrix}\cdot\begin{pmatrix}D1_i^{(0)}\\ D2_i^{(0)}\end{pmatrix} \tag{14-a}$$

We will show that only $D1_i^{(-1)}$ and $D1_i^{(0)}$ portions of vectors $D_i^{(-1)}$ and $D_i^{(0)}$ are independent variables: $D2_i^{(-1)}$ and $D2_i^{(0)}$ can be expressed through $D1_i^{(-1)}$ and $D1_i^{(0)}$. Equation (14-a) can be split in two:

$$F_{11}\cdot W_D\cdot D1_i^{(-1)}+Y_{11}\cdot D1_i^{(0)}+Y_{12}\cdot D2_i^{(0)}=-\Lambda_i\times W_D\cdot D1_i^{(0)} \tag{14-b}$$

$$F_{21} \cdot W_D \cdot D1_i^{(-1)} + Y_{21} \cdot D1_i^{(0)} + Y_{22} \cdot D2_i^{(0)} = 0 \qquad (14\text{-c})$$

Matrix (H_{SC} - $\varepsilon \times I$) is non-singular, and hence Y is non-singular as well. That, however, does not guarantee that its diagonal sub-block Y_{22} is non-singular. Singular Y_{22} is the pathological case mentioned earlier, when both Tomfohr-Sankey's and ours algorithms fail. Non-singularity of Y_{22} is the only requirement imposed by our algorithm on the Hamiltonian. In the following we assume Y_{22} to be non-singular. Thus, Eq.(14-c) can be used to express $D2_i^{(0)}$:

$$D2_i^{(0)} = -Y_{22}^{-1} \cdot F_{21} \cdot W_D \cdot D1_i^{(-1)} - Y_{22}^{-1} \cdot Y_{21} \cdot D1_i^{(0)} \qquad (14\text{-d})$$

Substituting Eq.(14-d) in Eq.(14-b) we obtain the first part of the eigenproblem for $\mathbf{T_{SC}}$:

$$W_D^{-1} \cdot \left(Y_{12} \cdot Y_{22}^{-1} \cdot F_{21} - F_{11}\right) \cdot W_D \cdot D1_i^{(-1)} + W_D^{-1} \cdot \left(Y_{12} \cdot Y_{22}^{-1} \cdot Y_{21} - Y_{11}\right) \cdot D1_i^{(0)} = \Lambda_i \times D1_i^{(0)} \qquad (15)$$

To obtain the second part we rewrite Eq.(13) in the sub-block form:

$$\begin{pmatrix} F_{11} & F_{12} \\ F_{21} & F_{22} \end{pmatrix} \cdot \begin{pmatrix} D1_i^{(0)} \\ D2_i^{(0)} \end{pmatrix} = \Lambda_i \times \begin{pmatrix} D1_i^{(-1)} \\ D2_i^{(-1)} \end{pmatrix} . \qquad (13\text{-a})$$

The upper portion of Eq.(13-a) is

$$F_{11} \cdot D1_i^{(0)} + F_{12} \cdot D2_i^{(0)} = \Lambda_i \times D1_i^{(-1)} \ . \qquad (13\text{-b})$$

After substitution of Eq.(14-c) we exclude $D2_i^{(0)}$ and obtain the second part of the eigen-problem:

$$-F_{12} \cdot Y_{22}^{-1} \cdot F_{21} \cdot W_D \cdot D1_i^{(-1)} + \left(F_{11} - F_{12} \cdot Y_{22}^{-1} \cdot Y_{21}\right) \cdot D1_i^{(0)} = \Lambda_i \times D1_i^{(-1)} \ . \qquad (16)$$

Combining Eqs.(15) and (16) we can write the entire eigenproblem in the sub-block form:

$$\mathbf{T_{SC}} \cdot D_i^{\times 2} \equiv$$

$$\left(\begin{array}{c|c} -F_{12} \cdot Y_{22}^{-1} \cdot F_{21} \cdot W_D & F_{11} - F_{12} \cdot Y_{22}^{-1} \cdot Y_{21} \\ \hline W_D^{-1} \cdot \left(Y_{12} \cdot Y_{22}^{-1} \cdot F_{21} - F_{11}\right) \cdot W_D & W_D^{-1} \cdot \left(Y_{12} \cdot Y_{22}^{-1} \cdot Y_{21} - Y_{11}\right) \end{array}\right) \cdot \begin{pmatrix} D1_i^{(-1)} \\ D1_i^{(0)} \end{pmatrix} = \Lambda_i \times \begin{pmatrix} D1_i^{(-1)} \\ D1_i^{(0)} \end{pmatrix}, \qquad (17)$$

where we defined $D^{\times 2}{}_i$ similarly to $C^{\times 2}{}_i$. It is easy to prove that $\mathbf{T_{SC}}$ has only non-zero eigenvalues. If we suppose the opposite, i.e. that $\Lambda_i = 0$, then, from Eq.(13) it follows that $D_i^{(0)} = 0$, because matrix F, which is the product of two unitary matrixes, is non-singular. Then Eq.(14) becomes:

$$F \cdot W \cdot D_i^{(-1)} = 0 \ , \qquad (18)$$

i.e. vector $W \cdot D1_i^{(0)} = 0$, which is possible only if $D1_i^{(0)} = 0$. This means that only trivial solution $D^{\times 2} = 0$ exists for $\Lambda_i = 0$.

Next let us show that the vector space spanned on $\{C^{\times 2}{}_i\}$ is reversibly mapped on $\{D^{\times 2}{}_i\}$. Equations (12) set up the mapping $\{C^{\times 2}{}_i\} \to \{D^{\times 2}{}_i\}$. From Eq.(12) it follows that

$$\begin{aligned} C_i^{(-1)} &= U \cdot D_i^{(-1)} \equiv U \cdot \begin{pmatrix} D1_i^{(-1)} \\ D2_i^{(-1)} \end{pmatrix}, \\ C_i^{(0)} &= V \cdot D_i^{(0)} \equiv V \cdot \begin{pmatrix} D1_i^{(0)} \\ D2_i^{(0)} \end{pmatrix} \quad . \end{aligned} \tag{19}$$

Using Eq.(14-d) we can eliminate $D2_i^{(0)}$ from the second Eq.(19) and hence express $C_i^{(0)}$ as the function of $D^{\times 2}{}_i$:

$$C_i^{(0)} = V \cdot \left(\begin{array}{c|c} 0 & I \\ \hline -Y_{22}^{-1} \cdot F_{21} \cdot W_D & -Y_{22}^{-1} \cdot Y_{21} \end{array} \right) \cdot \begin{pmatrix} D1_i^{(-1)} \\ D1_i^{(0)} \end{pmatrix} . \tag{20}$$

To express the first equation (19) as the function of $D^{\times 2}{}_i$ we need to obtain the analog of Eq.(14-d) for $D2_i^{(-1)}$. We start by dividing Schrödinger equation (9) over Λ_i:

$$\left(\tau_{SC} \cdot R_{SC}\right)^T \cdot C_i^{(-2)} + \left(H_{SC} - \varepsilon \times I\right) \cdot C_i^{(-1)} + \left(\tau_{SC} \cdot R_{SC}\right) \cdot C_i^{(0)} = 0 \tag{21}$$

After transforming Eq.(21) as

$$\left(H_{SC} - \varepsilon \times I\right) \cdot C_i^{(-1)} + \left(\tau_{SC} \cdot R_{SC}\right) \cdot C_i^{(0)} = -\Lambda_i^{-1} \times \left(\tau_{SC} \cdot R_{SC}\right)^T \cdot C_i^{(-1)} \quad , \tag{22}$$

we perform the substitutions given by Eq.(12) and write Eq.(22) in sub-block form analogously to Eq.(14-a):

$$\begin{pmatrix} Y_{11}^T & Y_{21}^T \\ Y_{12}^T & Y_{22}^T \end{pmatrix} \cdot \begin{pmatrix} D1_i^{(-1)} \\ D2_i^{(-1)} \end{pmatrix} + \begin{pmatrix} F_{11}^T & F_{21}^T \\ F_{12}^T & F_{22}^T \end{pmatrix} \cdot \begin{pmatrix} W_D & 0 \\ 0 & 0 \end{pmatrix} \cdot \begin{pmatrix} D1_i^{(0)} \\ D2_i^{(0)} \end{pmatrix} = -\Lambda_i^{-1} \times \begin{pmatrix} W_D & 0 \\ 0 & 0 \end{pmatrix} \cdot \begin{pmatrix} D1_i^{(-1)} \\ D2_i^{(-1)} \end{pmatrix} \tag{23}$$

The second line of the system (23) allows us to express $D2_i^{(0)}$ through $D1_i^{(-1)}$ and $D1_i^{(0)}$, i.e. through $D^{\times 2}{}_i$:

$$D2_i^{(-1)} = -\left(Y_{22}^T\right)^{-1} \cdot Y_{12}^T \cdot D1_i^{(-1)} - \left(Y_{22}^T\right)^{-1} \cdot F_{12}^T \cdot W_D \cdot D1_i^{(0)} \quad . \tag{24}$$

Now, combining Eqs.(19) and (24) we can express $C_i^{(-1)}$ through $D^{\times 2}{}_i$:

$$C_i^{(-1)} = U \cdot \left(\begin{array}{c|c} I & 0 \\ \hline -\left(Y_{22}^T\right)^{-1} \cdot Y_{12}^T & -\left(Y_{22}^T\right)^{-1} \cdot F_{12}^T \cdot W_D \end{array} \right) \cdot \begin{pmatrix} D1_i^{(-1)} \\ D1_i^{(0)} \end{pmatrix} . \tag{25}$$

Combining Eqs.(20) and (25) we define the mapping $\{D^{\times 2}{}_i\} \to \{C^{\times 2}{}_i\}$:

$$C_i^{\times 2} \equiv \begin{pmatrix} C_i^{(-1)} \\ C_i^{(0)} \end{pmatrix} = \begin{pmatrix} U & 0 \\ 0 & V \end{pmatrix} \cdot \left(\begin{array}{c|c} I & 0 \\ -\left(Y_{22}^T\right)^{-1} \cdot Y_{12}^T & -\left(Y_{22}^T\right)^{-1} \cdot F_{12}^T \cdot W_D \\ \hline 0 & I \\ -Y_{22}^{-1} \cdot F_{21} \cdot W_D & -Y_{22}^{-1} \cdot Y_{21} \end{array} \right) \cdot \begin{pmatrix} D1_i^{(-1)} \\ D1_i^{(0)} \end{pmatrix} \equiv X \cdot D_i^{\times 2} \quad . \qquad (26)$$

Since the mapping $\{C^{\times 2}{}_i\} \leftrightarrow \{D^{\times 2}{}_i\}$ is reversible, none of the physical solutions Λ_i is lost due to the transformation $\{C^{\times 2}{}_i\} \rightarrow \{D^{\times 2}{}_i\}$. Therefore transfer matrix $\mathbf{T_{SC}}$ in $\{D^{\times 2}{}_i\}$ space (Eq.(17)) contains all required eigenvalues. In the next section we will use mapping $\{C^{\times 2}{}_i\} \xleftrightarrow{X} \{D^{\times 2}{}_i\}$ given by Eq.(26) to build the transfer matrix **T** associated with the band-diagonal Hamiltonian structure.

Our construction of $\mathbf{T_{SC}}$ differs from Tomfohr-Sankey's construction in definition of $D_i^{(-1)} = U^T \cdot C_i^{(-1)}$ (Eq.(12)), which allows us to combine range sub-spaces of matrixes $\tau_{SC} \cdot R_{SC}$ and $(\tau_{SC} \cdot R_{SC})^{\mathrm{T}}$. Tomfohr and Sankey define $D_i^{(0)}$, as given by Eq.(12), but $D_i^{(-1)} = V^T \cdot C_i^{(-1)}$. According to their definition of vector $D_i^{(-1)}$ it contains both range and null-spaces of matrix $(\tau_{SC} \cdot R_{SC})^{\mathrm{T}}$, which results in larger transfer matrix and additional zero eigenvalues.

V. CONSTRUCTION OF T

To make explanation more visual we show **T** matrix construction for the seven band Hamiltonian given by Eq.(2); derivation of the general case is straightforward. Equations (6) and (3) can be combined in the following form:

$$\begin{aligned} &\left(H_3 R^3\right)^T c_i^{(-3)} + \left(H_2 R^2\right)^T c_i^{(-2)} + \left(H_1 R^1\right)^T c_i^{(-1)} + \\ &\left(H_0 - \varepsilon \times I\right) c_i^{(0)} + \left(H_1 R^1\right) c_i^{(1)} + \left(H_2 R^2\right) c_i^{(2)} = -\lambda_i \left(H_3 R^3\right) c_i^{(2)} \end{aligned} \qquad (6\text{-a})$$

Further, combination of Eqs.(3) and (6-a) can be written in the familiar matrix form:

$$\left(\begin{array}{c|c|c|c|c|c} 0 & I & 0 & 0 & 0 & 0 \\ \hline 0 & 0 & I & 0 & 0 & 0 \\ \hline 0 & 0 & 0 & I & 0 & 0 \\ \hline 0 & 0 & 0 & 0 & I & 0 \\ \hline 0 & 0 & 0 & 0 & 0 & I \\ \hline \left(H_3 R^3\right)^T & \left(H_2 R^2\right)^T & \left(H_1 R^1\right)^T & H_0 - \varepsilon \times I & H_1 R^1 & H_2 R^2 \end{array} \right) \cdot \begin{pmatrix} c_i^{(-3)} \\ c_i^{(-2)} \\ c_i^{(-1)} \\ c_i^{(0)} \\ c_i^{(1)} \\ c_i^{(2)} \end{pmatrix} = \lambda_i \begin{pmatrix} c_i^{(-3)} \\ c_i^{(-2)} \\ c_i^{(-1)} \\ c_i^{(0)} \\ c_i^{(1)} \\ -\left(H_3 R^3\right) \cdot c_i^{(2)} \end{pmatrix} \qquad (27)$$

We define $\{c^{\times 6}{}_i\}$ similar to $\{C^{\times 2}{}_i\}$ as the set of all possible vectors in the left-hand side of Eq.(27), which have the form of the Bloch functions (3) and satisfy Schrödinger equation (2). It is convenient to denote the matrix in the left-hand side of Eq.(27) as Q, and re-write it in the compact form:

$$Q \cdot c_i^{\times 6} = \lambda_i \times P \cdot c_i^{\times 6} \ , \tag{27-a}$$

where

$$P \equiv \begin{pmatrix} I & 0 & 0 & 0 & 0 & 0 \\ 0 & I & 0 & 0 & 0 & 0 \\ 0 & 0 & I & 0 & 0 & 0 \\ 0 & 0 & 0 & I & 0 & 0 \\ 0 & 0 & 0 & 0 & I & 0 \\ 0 & 0 & 0 & 0 & 0 & -\left(H_3 R^3\right) \end{pmatrix} . \tag{28}$$

If matrix H_3 is singular, some of the components of $c_i^{(2)}$ in the right hand side of Eq.(27) are "lost". Therefore the number of the components in the right-hand side is less than the size of the matrix, and the linear system (27) cannot be considered an eigenproblem in $\{c^{\times 6}{}_i\}$. This issue is resolved by expressing $\{c^{\times 6}{}_i\}$ through $\{D^{\times 2}{}_i\}$. Combining Eqs.(3) and (3-a) we relate $\{c^{\times 6}{}_i\}$ to $\{C^{\times 2}{}_i\}$:

$$\begin{pmatrix} R_{SC}^{-1} \cdot C_i^{(-1)} \\ C_i^{(0)} \end{pmatrix} = \begin{pmatrix} R^{-3} \cdot c_i^{(-3)} \\ R^{-2} \cdot c_i^{(-2)} \\ R^{-1} \cdot c_i^{(-1)} \\ c_i^{(0)} \\ R^{1} \cdot c_i^{(1)} \\ R^{2} \cdot c_i^{(2)} \end{pmatrix} \ , \tag{29}$$

which is convenient to present in the matrix form:

$$A \cdot \begin{pmatrix} C_i^{(-1)} \\ C_i^{(0)} \end{pmatrix} \equiv \left(\begin{array}{ccc|ccc} R^3 & 0 & 0 & 0 & 0 & 0 \\ 0 & R^2 & 0 & 0 & 0 & 0 \\ 0 & 0 & R^1 & 0 & 0 & 0 \\ \hline 0 & 0 & 0 & I & 0 & 0 \\ 0 & 0 & 0 & 0 & R^{-1} & 0 \\ 0 & 0 & 0 & 0 & 0 & R^{-2} \end{array}\right) \cdot \begin{pmatrix} R_{SC}^{-1} & 0 \\ 0 & I \end{pmatrix} \cdot \begin{pmatrix} C_i^{(-1)} \\ C_i^{(0)} \end{pmatrix} = \begin{pmatrix} c_i^{(-3)} \\ c_i^{(-2)} \\ c_i^{(-1)} \\ c_i^{(0)} \\ c_i^{(1)} \\ c_i^{(2)} \end{pmatrix} \ . \tag{30}$$

Thus $c^{\times 6}{}_i = A \cdot X \cdot D^{\times 2}{}_i$, and Eq.(27-a) can be rewritten in $\{D^{\times 2}{}_i\}$ space:

$$LHS \cdot D_i^{\times 2} = \lambda_i \times RHS \cdot D_i^{\times 2} \quad \text{, where}$$
$$LHS \equiv Q \cdot A \cdot X \tag{27-b}$$
$$RHS \equiv P \cdot A \cdot X \quad .$$

Matrixes *LHS* and *RHS* are rectangular: the number of rows equals the length of $c^{\times 6}{}_i$, which is larger than the number of columns equal to the length of $D^{\times 2}{}_i$. We add zero columns to *RHS* to convert it to the square matrix $(RHS \mid 0)$. $D^{\times 2}{}_i$ is appended zeros to fit the size of $(RHS \mid 0)$. We apply singular value decomposition to $(RHS \mid 0)$

$$(RHS \mid 0) = u \cdot w \cdot v^{\dagger} . \tag{31}$$

The energy ε, for which matrix **T** is constructed can be complex. In this case matrixes *Y* (Eq.(12)), *X* (Eq.(26)), *RHS*, *u*, and *v* are complex as well. That is the reason why we use Hermitian conjugation instead of transposition in Eq.(31). Equation (27-b) can be expressed in the sub-block form as

$$u^{\dagger} \cdot LHS \cdot D_i^{\times 2} = \lambda_i \times \begin{pmatrix} w_d & 0 \\ 0 & 0 \end{pmatrix} \cdot \begin{pmatrix} v_{11}^{\dagger} & v_{21}^{\dagger} \\ v_{12}^{\dagger} & v_{22}^{\dagger} \end{pmatrix} \cdot \begin{pmatrix} D_i^{\times 2} \\ 0 \end{pmatrix} . \tag{27-c}$$

Here the size of the square sub-block $v_{11}{}^{\dagger}$ is the same as the size of diagonal matrix w_d and equals the length of vector $D^{\times 2}{}_i$. Hence the size of the square sub-block $v_{22}{}^{\dagger}$ is the difference between the length of $c^{\times 6}{}_i$ and $D^{\times 2}{}_i$, i.e. twice the null-space of τ_{SC}. If we represent $u^{\dagger} \cdot LHS$ as

$$u^{\dagger} \cdot LHS = \begin{pmatrix} \left(u^{\dagger} \cdot LHS\right)_{Top} \\ \left(u^{\dagger} \cdot LHS\right)_{Btm} \end{pmatrix} ,$$

where $(u^{\dagger} \cdot LHS)_{Top}$ is square matrix of the same size as $D^{\times 2}{}_i$, Eq.(27-c) can be rewritten in the form of the two separate equations:

$$\begin{aligned} &\left(w_d \cdot v_{11}^{\dagger}\right)^{-1} \cdot \left(u^{\dagger} \cdot LHS\right)_{Top} \cdot D_i^{\times 2} = \lambda_i \times D_i^{\times 2} \\ &\left(u^{\dagger} \cdot LHS\right)_{Btm} \cdot D_i^{\times 2} = 0 \end{aligned} \quad . \tag{27-d}$$

From the previous section we know that all $\{\lambda_i\}$, which satisfy the first Eq.(27-d) are non-zero because all vectors $\{D^{\times 2}{}_i\}$ correspond to non-zero $\{\Lambda_i\}$, and $\lambda_i = \sqrt[M]{\Lambda_i}$. Hence matrix $(w_d \cdot v_{11}{}^{\dagger})^{-1} \cdot (u^{\dagger} \cdot LHS)_{Top}$ is non-singular and the first equation completely determines

$\{D^{\times 2}{}_i\}$ and $\{\lambda_i\}$ sets. The second equation does not contain any additional information and shall be disregarded. Therefore the final expression for the transfer matrix **T** is:

$$T = \left(w_d \cdot v_{11}^{\dagger}\right)^{-1} \cdot \left(u^{\dagger} \cdot LHS\right)_{Top} \tag{32}$$

It is interesting to note that since $\Lambda_i = \lambda_i{}^{\mathrm{M}}$, and both **T** and $\mathbf{T_{SC}}$ have the same set of eigenvectors $\{D^{\times 2}{}_i\}$, $\mathbf{T_{SC}} = \mathbf{T}^{\mathrm{M}}$. That is indeed confirmed by numerical tests.

VI. ALGORITHM SUMMARY

We have designed the algorithm for the construction of the transfer matrix **T**. For any given real or complex energy ε the eigenvalues of the transfer matrix $\lambda_i \equiv Exp[i\,k_i]$ determine all possible $\{k_i\}$ and $\{C_i\}$, which satisfy the Schrödinger equation in *k*-representation for 1-D structure with either translational or screw symmetry:

$$H\left[k_i\right] \cdot C_i = \varepsilon \times C_i$$

$$H\left[k\right] = h^{(0)} + \sum_{n=1}^{M}\left(\left(h^{(n)}\right)^{T}\ Exp\left[-i\,k\,n\right] + h^{(n)}\ Exp\left[i\,k\,n\right]\right)$$

The input data for the transfer matrix construction are the unit cell Hamiltonian sub-blocks and the unit cell orbital rotation matrix. From these matrixes we generate the tri-block-diagonal supercell structure as given by Eq.(2). Then, we perform the singular value decomposition of $\tau_{SC} \cdot R$ (Eq.(10)). From the matrixes resulting from the singular value decomposition we construct matrix *X*, which maps $\{D^{\times 2}{}_i\}$ to $\{C^{\times 2}{}_i\}$. After that we construct matrixes *Q* and *P* from the unit cell Hamiltonian sub-blocks (Eqs.(27-28)), and matrix *A* from the orbital rotational matrix (Eq.(30)). Finally we build **T** matrix (Eqs.(27-b,c,d), (31) and (32)). The solution of **T** eigenproblem gives us $\{D^{\times 2}{}_i\}$ and $\{\lambda_i\}$ sets. The state vectors in atomic orbital representation are obtained as $c^{\times 6}{}_i = A \cdot X \cdot D^{\times 2}{}_i$. The eigenvectors $c^{(0)}{}_i$ of Hamiltonian (1-a) are extracted as the appropriate portions of $c^{\times 6}{}_i$.

VII. NANO-TUBE CONDUCTANCE vs. BENDING ANGLE

We used the Landauer's approach to study small voltage conductance of (10,7) and (8,8) nano-tubes with respect to the bending angle. The number of atoms in the bent portions of (10,7) and (8,8) nano-tubes was 1428 and 1344 respectively. Bending angle

ranges from 0° to 120° with the angle increment 0.833°. Structure relaxation was performed using analytic potential[6], and the environment-dependent tight-binding[3] with its self-consistent extension[4,5] were used to construct the Hamiltonian. Self-consistent electron density was computed for (10,7) nano-tube for the three values of the bending angle (Figs.1-3): (1) right before the conductance drop, (2) immediately after the conductance drop, and (3) for the maximum bending angle. Since both self-energy and transfer matrix algorithms are equally applicable to real and complex energies, the electron density was obtained by the contour integration in the upper complex energy half-plane.[7] Taking advantage of the system's linear structure we subdivided it into super-cells, which interact only with their nearest neighbors. The self-energy propagation described in the previous paper was applied to compute the Green's function diagonal sub-blocks corresponding to each super-cell. This leads to the linear scaling of computational expenses with the length of the bent portion of the nano-tube. The variant of Broyden's method[8] was used to accelerate self-consistency convergence.

Because the open boundary conditions assume that the Fermi level equals the Fermi level of the infinitely long nano-tube, the total charge of the bent portion of the nano-tube can differ from zero. For configurations (1), (2), (3) we found that the bent region has the small positive total charge equal respectively to 0.114, 0.108, 0.079 of electron fraction.

We compute the Landauer's conductance $C[\varepsilon]$ exactly the same way as it is described in the previous paper. Although the conductance vs. energy dependence for the self-consistent computation is substantially different from the non-self-consistent case, the difference for the total current

$$I[V] = \int_{-V/2-20kT}^{+V/2+20kT} C[\varepsilon]\ \left(f[\varepsilon - (\mu_0 + V/2)] - f[\varepsilon - (\mu_0 - V/2)] \right) d\varepsilon\ , \qquad f[x] = \left(1 + Exp[x/kT]\right)^{-1} \tag{33}$$

between self-consistent and non-self-consistent cases is reasonably small (Fig. 3). Based on that finding we perform all other computations by using non-self-consistent model.[3] For applied bias less than 0.4 V and room temperature Eq.(33) gives almost linear I-V dependence (cf. insert in Fig. 4) for the entire range of bending angles.

To better understand the abrupt decrease of the conductance (Fig. 4) and the associated current (Fig. 3) caused by a small angle increment it is convenient to monitor the evolution of the local density of states at the kink region. Since most of the state density near the Fermi level is contributed by π-orbitals, which are aligned in x-z plane at the kink area (cf. Figs. 1,2), one needs to monitor the change of Im[$G_{x,x}$], Im[$G_{z,z}$], and Im[$G_{x,z}$] for the atoms at the kink region. To obtain the π-density from these three quantities one needs to rotate the coordinate system in such way that only one diagonal component, e.g. Im[$G_{x,x}$], remains non-zero. In practice, however, it appears that for the problem in hand Im[$G_{x,z}$] has little effect on the local π-density, and it can be approximated by $\pi^{-1}(\mathrm{Im}[G_{x,x}]^2 + \mathrm{Im}[G_{z,z}]^2)^{1/2}$. From Fig. 5 one can see that as the opposite nano-tube walls at the kink region approach each other, the abrupt rearrangement of local electron configuration takes place. The transition from configuration (1) to configuration (2) corresponds to the severe alteration of the local π-density, which becomes strongly dissimilar to the π-density in the perfect nanotube. That manifests the appearance of the local states, which is consistent with the earlier findings.[9-10] The localized states cause the strong scattering and lower the conductance. At the same time the local π-density near the Fermi level in the left column of Fig. 5 is represented by smooth functions, which are analogous to the π-density of the ideal tube. Hence no well defined localized states exist in configuration (1), and only little scattering occurs.

The diameters of (10,7) and (8,8) nano-tubes are almost the same, and if one disregards the tiny band gap of the (10,7) tube, which is smaller than kT, both tubes can be considered metallic with two conducting channels in the vicinity of the Fermi level. Provided these similarities, the difference in the current vs. angle plots (Fig. 3) can originate only from the different mutual orientation of the kink and the nano-tube's roll vectors. Because the Lippmann-Schwinger equation for 1-D systems can be solved exactly, one can investigate the effect of the kink symmetry on the intra- and inter-channel scattering amplitudes. We reserve the examination of this topic for the future publication.

VIII. SUMMARY

We presented the fast and numerically robust algorithm for the construction of the transfer matrix associated with the arbitrary one-dimensional structure possessing translational or screw symmetry. The algorithm is capable of handling an arbitrary type of singularities in the Hamiltonian matrix. The transfer matrix algorithm is the essential part of the algorithm used for the computation of Green's functions and self-energies. The algorithm was applied to simulate the self-consistent electron densities and conductances for the (10,7) and (8,8) infinite bent nano-tubes. The conductances of both nano-tubes appear to be very insensitive to bending until the bending angle reaches 60°. At that point the interaction of the π-electrons from the opposite walls of the nano-tube in the kink region causes the abrupt decrease of the nano-tube conductance. Further bending up to 120° does not have a substantial effect on the conductance, which constitutes about 25% from the ideal conductance for the (10,7) nano-tube and about 70% for the (8,8) nano-tube.

REFERENCES:

[1] Yia-Chung Chang and J.N. Schulman, Phys. Rev. B, **25**, 3975, (1981).

[2] J.K. Tomfohr and O.F. Sankey, Phys. Rev. B, **65**, 245105, (2002).

[3] Tang, M.S., Wang, C.Z., Chan, C.T., and Ho, K.M. (1996) "Environment-dependent tight-binding potential model", Phys. Rev. B **53**, 979; (1996), **54**, 10982.

[4] D.A. Areshkin, O.A. Shenderova, J.D. Schall, and D.W. Brenner, "Self-consistent tight binding model adapted for hydrocarbon systems", Molecular Simulation **31** (8), 585 (2005).

[5] D.A. Areshkin, O.A. Shenderova, J.D. Schall, and D.W. Brenner, "Self-consistent tight binding model adapted for hydrocarbon systems: Application to field emission from nanodiamond clusters.", J. Phys.: Condens. Matter **16** 6851 (2004).

[6] D.W. Brenner, "Empirical potential for hydrocarbons for use in simulating the chemical vapor deposition of diamond films", Phys. Rev. B **42**, 9458 (1990); **46**, 1948 (1992).

[7] M. Brandbyge, J.-L. Mozos, P. Ordejon, J. Taylor, and K. Stokbro, "Density-functional method for nonequilibrium electron transport", Phys. Rev. B **65**, 165401 (2002).

[8] D.D. Johnson, "Modified Broyden's method for accelerating convergence in self-consistent calculations", Phys. Rev. B **38**, 12807 (1988).

[9] M.S.C. Mazzoni and H. Chacham, "Atomic restructuring and localized electron states in a bent carbon nanotube: A first-principles study", Phys. Rev. B **61**, 7312 (2000).

[10] L.F. Chibotaru, S.A. Bovin, and A. Ceulemans, "Bend-induced insulating gap in carbon nanotubes", Phys. Rev. B **66**, 161401(R) (2002).

FIGURES

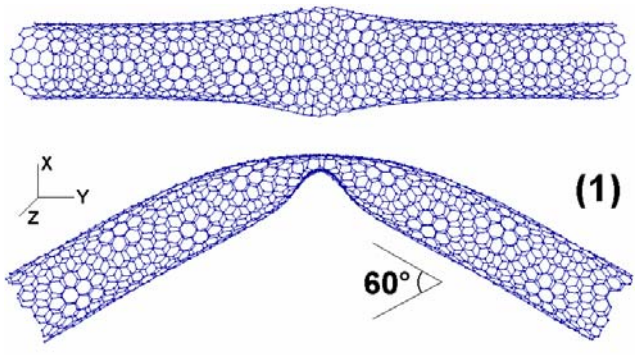

Figure 1

Top and side views of the (10,7) nano-tube for the bending angle φ = 60°, which corresponds to point (1) in Fig.3. The increase of φ by 0.83° brings the system to the low-conducting state denoted as point (2) in Fig.3. There is no visually noticeable difference between the configurations with φ = 60° and φ = 60.83° so we do not show the latter.

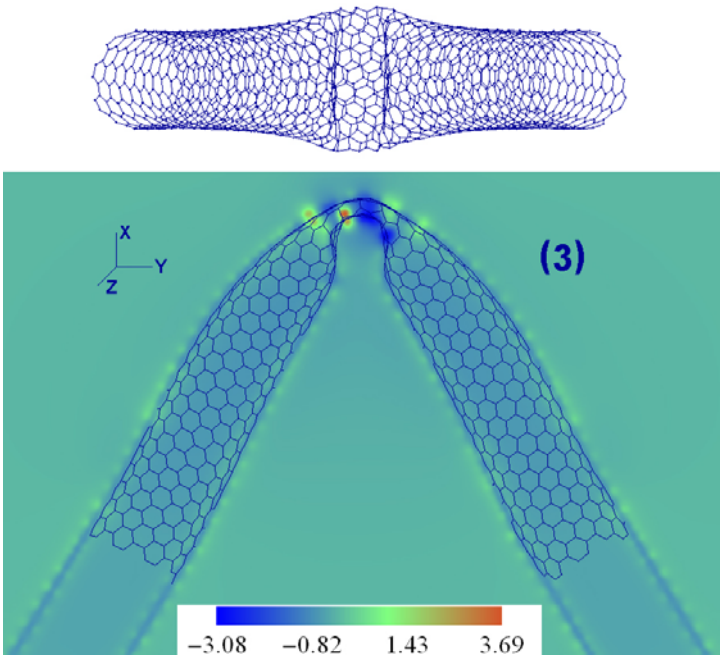

Figure 2

Top and side views of the (10,7) nano-tube for the maximum bending angle φ = 121.7°, which corresponds to point (3) in Fig.3. Color-coded plot represents the self-consistent Coulomb potential in the bending plane passing through the center of mass. For clarity only the part of the system lying above the plane is shown. The Coulomb potential is produced by the electron density associated with the finite bent portion of the nanotube and the semi-infinite periodic portions of the nano-tube (not shown in the figure).

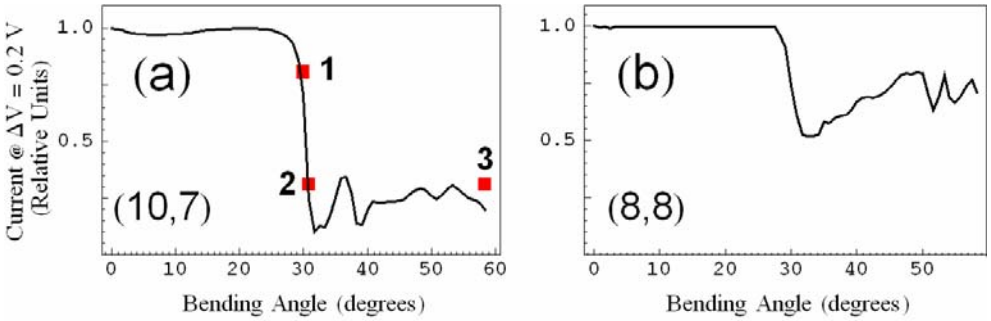

Figure 3

The relative change of the current as the function of the bending angle at 0.2 V bias voltage. Squares in pane (a) denote current values computed using self-consistent environment-dependent tight-binding Hamiltonian.

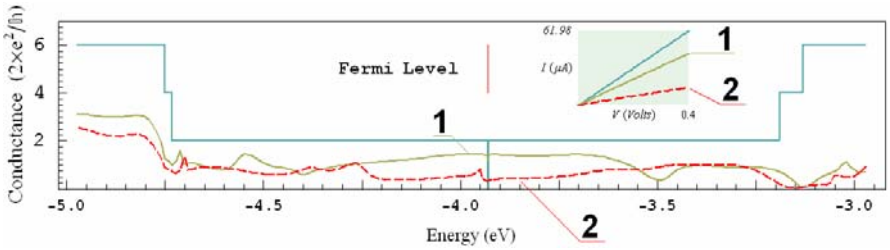

Figure 4

Energy dependence of the (10,7) nano-tube conductance. Curves 1 and 2 correspond respectively to the bending angles φ = 60° and φ = 60.83° denoted by points (1) and (2) in Fig. 3. Energy dependence for the conductance of the perfect nano-tube is plotted for reference. The insert shows the I-V plots for φ = 60° and φ = 60.83°; the top line is the I-V dependence for the perfect nano-tube.

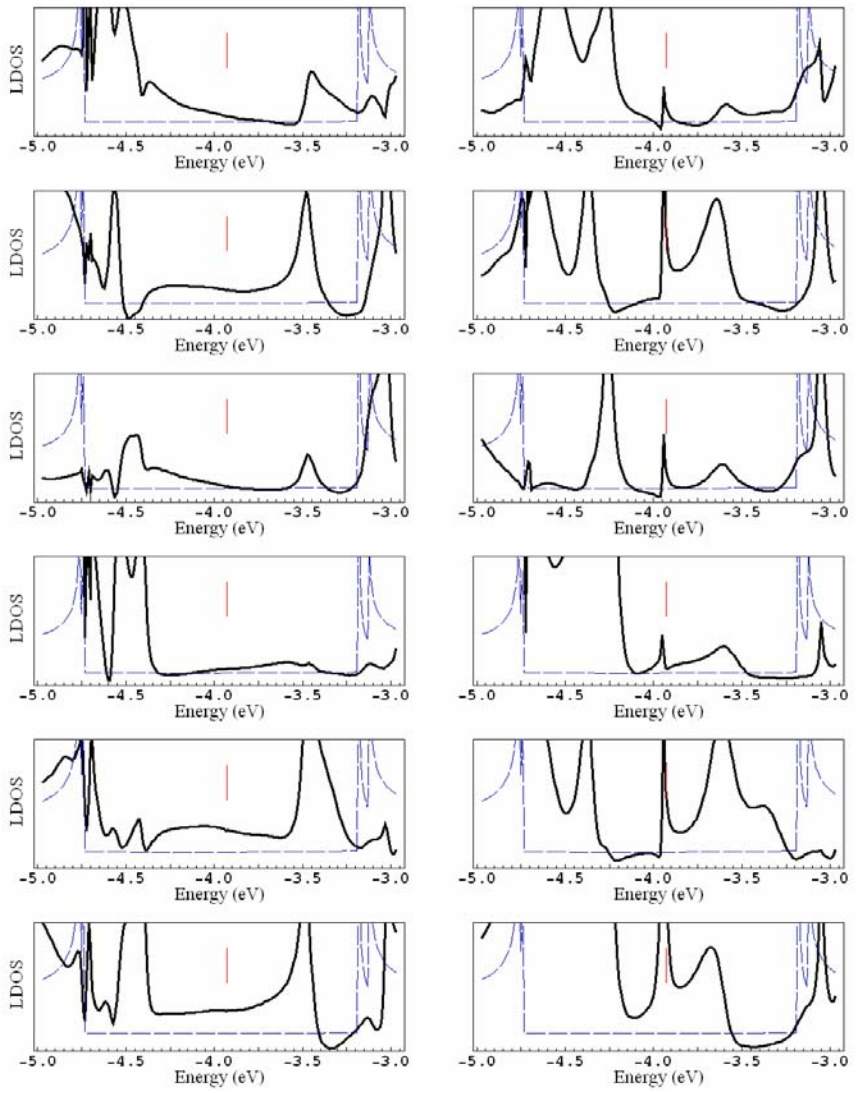

Figure 5

Local DOS associated with π-orbitals: $\mathrm{LDOS}_\pi = \pi^{-1}(\mathrm{Im}[G_{x,x}]^2 + \mathrm{Im}[G_{z,z}]^2)^{1/2}$ plotted for six atoms at the kink region of (10,7) nano-tube right before (φ = 60°, left column) and immediately after (φ = 60.83°, right column) the onset of the critical angle. Vertical mark indicates the Fermi level. Dashed line denotes LDOS_π for the perfect (10,7) nano-tube. The spikes at the Fermi level appearing in the right column indicate the emergence of the localized state.